

IMAGE PROCESSING

https://doi.org/10.1070/QEL17039

On the possibility of a significant improvement in the quality of a quantum ghost image by registering an additional image in the object channel

D.A. Balakin, A.V. Belinsky

Abstract. **A modification of the classical scheme of the quantum ghost image formation is considered, in which an image of the object under study is formed and recorded in the object channel. This image is used together with the ghost image to construct an estimate of the transparency distribution of the object. It is shown that this technique reduces the image quality worsening associated with the non-unit quantum efficiency of the sensors, even when the quantum image obtained in the object channel is additionally distorted by noise due to photons that did not interact with the object.**

Keywords: *ghost images, measurement reduction, quantum detector efficiency, entangled photons.*

1. Introduction

One of the important arguments in favour of using quantum ghost images is to provide the most sparing lighting conditions for the studied object when the effect of radiation on the object (sometimes irreversible) is minimal [1]. This is especially important when irradiating living objects, e. g., by X-rays.

In the classical scheme of the ghost imaging in the object arm (where the studied object is located), radiation is detected by an integrating detector, i. e., a single-element photodetector that intercepts the entire beam of radiation that penetrates through the object of study or is reflected from it (Fig. 1). In this case, of course, no image is obtained. The image is formed in another channel due to the strong correlation between the photons in these two channels. With fixed characteristics of the optical scheme and given information about the object of study available to the researcher, the minimum illumination of the object at which acceptable image quality is achievable can only be reduced by increasing the quantum efficiency of the detectors. However, such forcing not only has finite reserves, but also leads to growing technical difficulties and financial costs. Moreover, if ordinary images only require registration of the photon interacting with the object, the formation of ghost images requires registration of a pair of photons, i. e., the average number of registered photons is proportional to the square of quantum efficiency.

D.A. Balakin, A.V. Belinsky Faculty of Physics, M.V. Lomonosov Moscow State University, Vorob'evy gory, 119991 Moscow, Russia; e-mail: balakin_d_a@physics.msu.ru, belinsky@inbox.ru

Received 9 April 2019; revision received 11 June 2019
Kvantovaya Elektronika **49** (10) 967–973 (2019)
Translated by V.L. Derbov

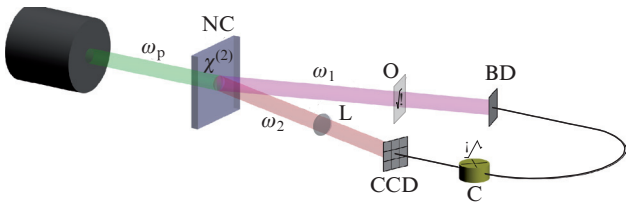

Figure 1. Classical scheme of ghost imaging:
(NC) nonlinear crystal; (O) object; (BD) bucket detector in the object channel; (L) collecting lens; (CCD) matrix of photodetectors in the reference channel; (C) intensity correlator; ω_p is the frequency of the quanta of the pump beam; ω_1 and ω_2 are the frequencies of entangled photon pairs (the beams diverge due to the use of a noncollinear process of parametric scattering).

We offer a new schematic solution that ensures, on the one hand, the safety of the object of study by reducing the light intensity, and on the other hand, improving the image quality. Moreover, the increase in the signal-to-noise ratio characteristic of ghost images generated by the coincidence scheme remains valid, i. e., it is possible to combine the advantages of the ghost image method with the advantages of the ordinary image formation.

Consider Fig. 2. In the object channel, as in the reference channel, instead of an integrating detector, a photodetector array is used, on which an ordinary image of the object under study is formed by means of an optical lens. In the case of X-ray irradiation, the matrix is placed directly behind the object, since in the X-ray region only reflective optical systems with large angles of incidence work well, and the image quality leaves much to be desired.

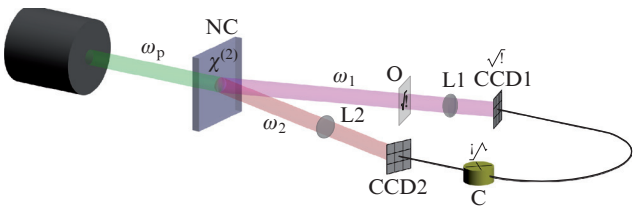

Figure 2. Proposed scheme for the formation of a pair of quantum images:
(NC) nonlinear crystal; (O) object; (L1, L2) optical lenses; (CCD1, CCD2) photodetector arrays in the object and reference channels; (C) intensity correlator; ω_p is the frequency of the quanta of the pump beam; ω_1 and ω_2 are the frequencies of entangled photon pairs (the beams diverge due to the use of a noncollinear process).

Thus, in the considered scheme two quantum images are registered, an ordinary image and a ghost one. Their subsequent computer processing makes it possible to reduce the minimum required number of photons penetrating through the object and to improve image quality. Note that the proposed scheme differs from the difference measurement scheme (see, e. g., [2]), because, in contrast to the latter, the obtained images are not processed by calculating their difference. This means, in particular, that the rigorous condition of the absolute identity of the detectors in the object and reconstruction channels is removed. In addition, due to the radically different operating principles of our scheme and difference ones, the layouts of their optical systems differ too.

2. Measurement reduction method

When illuminating an object with a minimum number of photons, the efficiency of mathematical methods and measurement processing algorithms should be such that they not only provide a minimum error, but also allow all information about the object available to the researcher to be used. This can be achieved using the mathematical method of measurement reduction and the algorithms that implement it.

Consider a typical measurement scheme in which a measured signal f, belonging to the Euclidean space $\mathcal{F}$, is formed at the input of the measuring transducer (MT) [3]. The MT transforms the signal f into a signal belonging to the Euclidean space $\mathcal{X}$

$$\xi = Af + v, \tag{1}$$

where $A: \mathcal{F} \to \mathcal{X}$ is an operator that simulates physical processes in the MT that determine the conversion of f into the signal Af; below it denotes the simulated MT itself; and v is the error (measurement noise). The measurement result depends on the characteristics of the measured object, interacting with the MT and distorted by the measurement, and the researcher, as a rule, is interested in the characteristics of the object not distorted by the measurement. Their relation is modelled by an ideal MT specified by the operator $U: \mathcal{F} \to \mathcal{U}$, the input of which receives the same signal as the input of MT A, but at its output, the signal Uf corresponds to the object characteristic interesting for the researcher. The reduction problem is to find the reduction operator R_* for which $R_*\xi$ is the most precise version of Uf; the reduction operator R_* is synthesised in a computational converter. If in Eqn (1) f is a priori an arbitrary vector, and v is a random vector taking values in the space $\mathcal{X}$ and having mathematical expectation $\mathrm{E}v = 0$ and non-degenerate covariance operator Σ_v: $\forall x \in \mathcal{X}\ \Sigma_v x = \mathrm{E}v(x,v)$, then the linear reduction operator $R_* : \mathcal{X} \to \mathcal{U}$ is defined as the operator minimising the maximum-in-f mean-square error of interpreting $R\xi$ as Uf:

$$h(R,U) = \sup_{f\in\mathcal{F}} \| R\xi - Uf \|^2.$$

This error is minimal [3] for

$$R_* = U(A^\dagger \Sigma_v^{-1} A)^{-1} A^\dagger \Sigma_v^{-1} \tag{2}$$

and is defined by the expression

$$h(R_*, U) = \mathrm{tr} U(A^\dagger \Sigma_v^{-1} A)^{-1} U^\dagger, \tag{3}$$

if $U(I - A^- A) = 0$, otherwise the error (3) is infinite. Here I is the unit operator; A^- is the operator pseudo-inverse to A; and the symbol † means the Hermitian conjugation.

Let the researcher be interested in the distribution of the transparency of the object. The pixel transparency values belong to a unit segment. This is taken into account in the measurement reduction by projecting the estimate onto the set $[0,1]^{\dim \mathcal{U}}$ [4–6]. Namely, the estimate is defined as a fixed point of the mapping combining the linear reduction result $R_*\xi$ and some estimate $\hat{u}$ of the transparency distribution as uncorrelated results of the 'main' and dummy measurements followed by projection onto the set $[0,1]^{\dim \mathcal{U}}$ while minimising the Mahalanobis distance $\| \Sigma_{R_*\xi}^{-1/2} \|$ associated with the covariance operator $\Sigma_{R_*\xi} = U(A^\dagger \Sigma_v^{-1} A)^{-1} U^\dagger$ of the linear reduction estimate. Besides that, the researcher is aware that the transparencies of adjacent pixels, as a rule, differ slightly. This information is often formalised [7–11] by the sparsity of the transparency distribution as a vector Uf in a given basis, i. e., as information that a significant fraction of the vector Uf components is zero in this basis.

In Refs [12, 13], a reduction algorithm was proposed that allows the researcher to take such information into account when processing multiplexed quantum ghost images. The algorithm is based on testing statistical hypotheses about the equality (or inequality) of the estimate components in the selected basis to zero. The result depends on the algorithm parameter τ, the level of the criterion used in the test of hypotheses. The choice of this parameter is determined by a compromise acceptable to the researcher between noise reduction and image distortion. To select the value of τ, the researcher can simulate the registration of a test image containing the required details, and use the maximum value of τ at which they are preserved. A similar method for choosing the regularisation parameter was proposed in Ref. [14], where the result of a Gaussian blur of the image corresponding to the lack of sparsity information was taken as a test image. An alternative way is to set τ by comparing the results of reduction for various values of τ and using available information about noise [15].

3. Influence of the quantum efficiency of detectors on the measurement scheme

Let the CCD matrices in the object and reconstruction channels be similar and described by the operator A_0. This assumption is made to simplify the formulas below (an arbitrary difference in the instrument functions requires considering infinite-dimensional spaces $\mathcal{F}$ and $\mathcal{X}$) and is not fundamental. A more detailed study of the effect of differences in the instrument functions of the sensors in the object and reconstruction channels, caused primarily by diffraction [16–18], is a subject of further studies.

With the unit quantum efficiency of the detectors in the object and reconstruction channels, the signal measurement scheme (1) takes the form

$$\xi = \begin{pmatrix} \xi_0 \\ \xi_1 \end{pmatrix} = \begin{pmatrix} A_0 \\ A_0 \end{pmatrix} nf + \begin{pmatrix} v_{\mathrm{img}} + v_\varepsilon \\ v_{\mathrm{img}} \end{pmatrix},$$

where ξ_0 is the result of measurement using the CCD matrix in the object channel; ξ_1 is the measurement result of the generated quantum ghost image; v_{img} is the error caused by the registration of quantum images; v_ε is the error of the

quantum image formed in the object channel due to noise photons; and n is the average number of photons illuminating the object. Note that during ghost imaging, noise photons are suppressed by the coincidence scheme if its response time is sufficiently short (see the comparison of quantum image formation schemes in Ref. [7]); otherwise, a term analogous to v_ε appears in the expression for the error of the quantum ghost image. The covariance error operator has the form

$$\Sigma_v = \begin{pmatrix} A_0 S(f) A_0^\dagger + \Sigma_{v_\varepsilon} & A_0 S(f) A_0^\dagger \\ A_0 S(f) A_0^\dagger & A_0 S(f) A_0^\dagger \end{pmatrix}$$

$$= \begin{pmatrix} 1 & 1 \\ 1 & 1 \end{pmatrix} \otimes A_0 S(f) A_0^\dagger + \begin{pmatrix} \Sigma_{v_\varepsilon} & 0 \\ 0 & 0 \end{pmatrix}, \quad (4)$$

where the operator $S(f)$ is determined by the variances and covariances of the photocounts. For example, if the statistics of photocounts is Poissonian, then $S(f) = n\,\mathrm{diag} f$. Hereinafter, $\mathrm{diag} q$ is a matrix whose diagonal elements are equal to the corresponding elements of the matrix q and the rest ones are zero; the symbol $\otimes$ denotes the Kronecker product. In this case, the registration of the spatial distribution of the radiation intensity in the object channel does not allow one to improve the reduction quality (the result of this measurement does not affect the result of the reduction).

With the detector efficiency in the object channel η_0 and the detector efficiency in the reconstruction channel η_1, the measurement scheme takes the form

$$\xi = \begin{pmatrix} \xi_0 \\ \xi_1 \end{pmatrix} = \begin{pmatrix} \eta_0 A_0 \\ \eta_0 \eta_1 A_0 \end{pmatrix} nf + \begin{pmatrix} v_{\mathrm{img}} + v_0 + v_\varepsilon \\ v_{\mathrm{img}} + v_0 + v_1 \end{pmatrix},$$

where the additional errors v_0 and v_1 are due to missing part of photons by the detectors in the object and reconstruction channels, respectively. The covariance error operator in this case has the form

$$\Sigma_v = \eta_0^2 \begin{pmatrix} 1 & \eta_1 \\ \eta_1 & \eta_1^2 \end{pmatrix} \otimes A_0 S(f) A_0^\dagger + \eta_0^2 \begin{pmatrix} \Sigma_{v_\varepsilon} & 0 \\ 0 & 0 \end{pmatrix}$$

$$+ \begin{pmatrix} \eta_0(1-\eta_0) & \eta_0(1-\eta_0)\eta_1 \\ \eta_0(1-\eta_0)\eta_1 & \eta_0\eta_1(1-\eta_0\eta_1) \end{pmatrix} \otimes \mathrm{diag}(A_0 f), \quad (5)$$

where the first two terms are of the same origin as in Eqn (4), but they are smaller because of the reduction of the average number of photocounts, and the last term is directly related to the non-unit efficiency of the sensors.

Since the linear reduction operator has the form (2) and the error in the reduction estimation in the absence of additional information is determined by Eqn (3), the gain determined by the registration of the image on the object channel is

$$\Delta h = \eta_0^{-2} \mathrm{tr} U \Big\{ \eta_0 \eta_1^{-1} \{ A_0^\dagger [\eta_0 \eta_1 A_0 S(f) A_0^\dagger + (1 - \eta_0\eta_1)$$

$$\times \mathrm{diag}(A_0 f)]^{-1} A_0 \}^{-1} - \left[(A_0^\dagger \eta_1 A_0^\dagger) \Sigma_v^{-1} \begin{pmatrix} A_0 \\ \eta_1 A_0 \end{pmatrix} \right]^{-1} \Big\} U^\dagger, \quad (6)$$

where the operator Σ_v is defined by Eqn (5). Figure 3 shows the relative gain in the average number of photons illuminating the object, depending on the quantum efficiency of the sensors and the relative average number of noise photons (relative to the average number of illuminating photons used to record only the ghost image) in the case of the same sensor efficiencies in the object and reconstruction channels. However, we have also considered a more general case. The gain is defined as the ratio of the decrease in the average number of photons required to illuminate the object to the average number Δn of illuminating photons in the traditional scheme with the error of the reconstructed image being constant. It is assumed that the number of noise photons n_ε decreases proportionally to n. As expected, the gain increases monotonically with a decrease in the number of noise photons and with a decrease in the quantum efficiency of the sensors $\eta = \eta_0 = \eta_1$. In the absence of noise photons, the relative gain is $1 - \eta$. If there is additional information, the gain, as a rule, decreases, with its sign unchanged, because at the same time both compared errors decrease, the larger one being reduced to a greater extent.

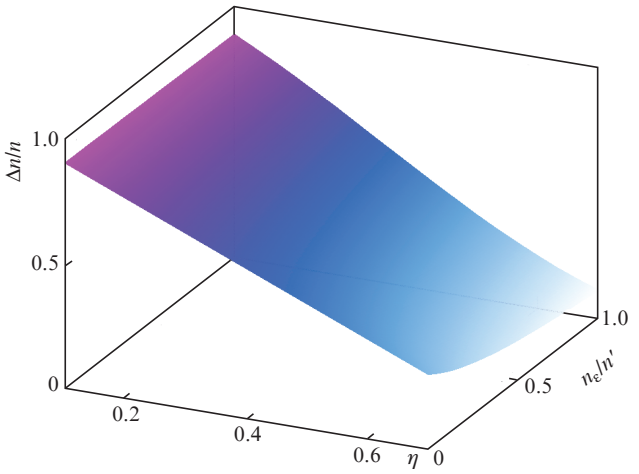

Figure 3. Relative gain $\Delta n/n$ in the average number of photons illuminating the object as a function of the quantum efficiency of the sensors $\eta = \eta_0 = \eta_1$ and the relative average number of noise photons n_ε/n '(relative to the average number n' of illuminating photons used to record only the ghost image).

Note that in the case of different quantum efficiencies of the sensors in the object and reference channels, it is more preferable to place the sensor having greater efficiency in the object channel, because, as seen from Eqns (5) and (6), this does not change the noise level of the recorded ghost image, which is affected by the product of the efficiencies, but reduces the noise level of the image in the object channel.

4. Results of computer simulation

Figures 4–11 show the results of computer simulation and subsequent processing of quantum images by the method of measurement reduction using the algorithm described in Refs [12, 13]. In the simulation, it was assumed that similar matrices are located in both channels, the sensors in which have a size three times greater than the size of the object pixel. In the

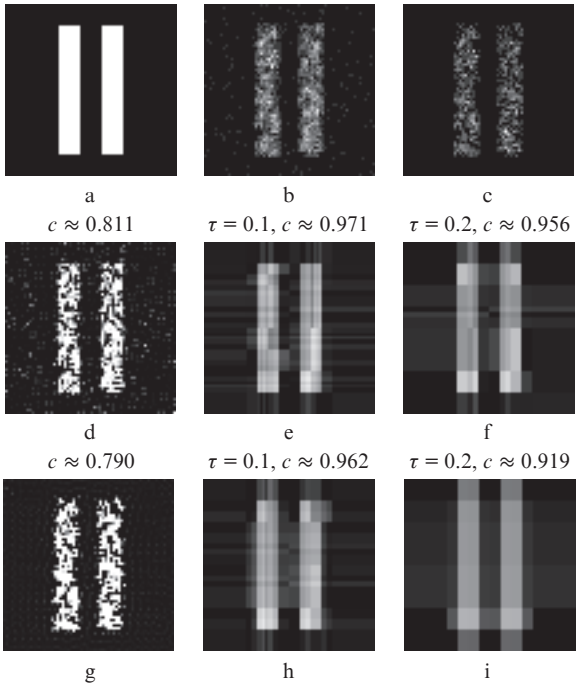

Figure 4. Quantum images of (a) the object recorded in (b) the object and (c) reconstruction channels and the results of their processing by the reduction method: processing of both images (d) in the absence of sparsity information and (e, f) in the presence of such information for two values of the algorithm parameter τ, as well as (g–i) similar processing of ghost images only. The average number of photons is 1 photon per pixel for illumination and 0.1 photon per pixel for noise.

case illustrated by Fig. 4, each pixel of the object is illuminated on average by 1 photon, the average number of noise photons that do not interact with the object but fall on the matrix in the object channel is 0.1 photons per object pixel, and the quantum efficiencies of the sensors in the object and reconstruction channels are 0.4. In Fig. 5, the average number of illuminating photons is reduced to 0.7 photons per pixel with a proportional decrease in the number of noise photons. In Figs 6 and 7, the quantum efficiencies of the sensors in one of the channels are reduced to 0.2, and in Fig. 8 the same reduction of efficiency to 0.2 in all the sensors is considered. Figures 9 and 10 show the simulation results with a decrease and increase in the number of noise photons by a factor of 10. Figure 11 shows the results of modelling the illumination and recording images for another object and with a different basis, using which the sparsity information is formalised. Figures 4–11 show the values of the numerical characteristic of the overlap $c(\hat{u},u) = (\hat{u},u)/(\|\hat{u}\|\|u\|)$ of the estimate $\hat{u}$ and the transparency distribution u.

As noted above, the parameter τ of the algorithm reflects a compromise acceptable for the researcher between noise suppression and image distortion. The larger the value of τ, the more noise is suppressed, but the distortion of image details also gradually increases (compare, e. g., Figs 4h and 4i, where the gap image is blurred with increasing τ). The value $\tau = 0$ corresponds to the absence of both additional noise suppression associated with the use of sparsity information about the transparency distribution and image distortion, i. e., it is equivalent to the absence of sparsity information about the transparency distribution of the object. The val-

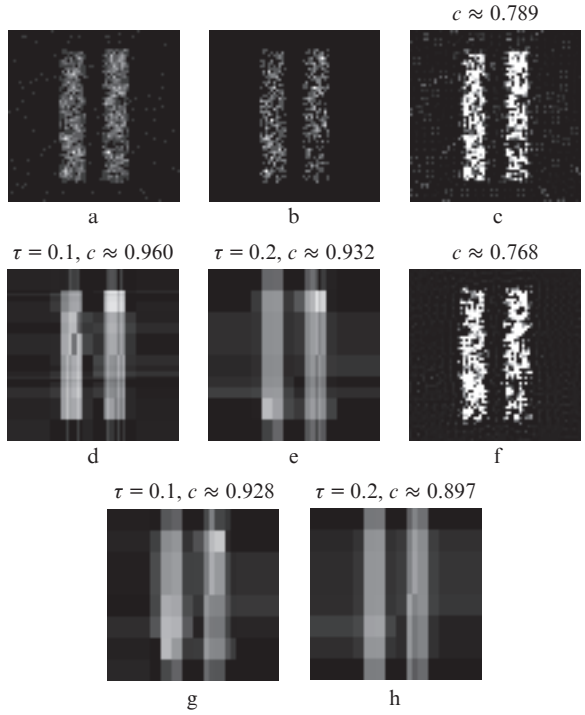

Figure 5. Quantum images of the object in Fig. 4a, recorded in (a) the object and (b) reconstruction channels, and the results of their processing by the reduction method: processing both images (c) in the absence of sparsity information and (d, e) in the presence of such information, as well as (f–h) similar processing of a ghost image only. The average number of photons is 0.7 photons per pixel for illumination and 0.07 photons per pixel for noise.

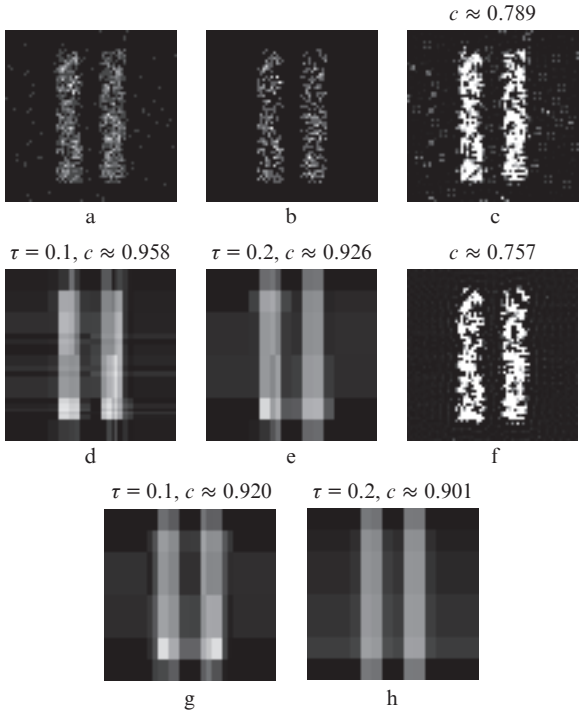

Figure 6. Quantum images of the object in Fig. 4a, recorded in (a) the object and (b) reconstruction channels, and the results of their processing by the reduction method: processing of both images (c) in the absence of sparsity information and (d, e) in the presence of such information, as well as (f–h) similar processing of a ghost image only. In contrast to Fig. 4, the quantum efficiencies of the detectors are 0.2 in the object channel and 0.4 in the reconstruction channel.

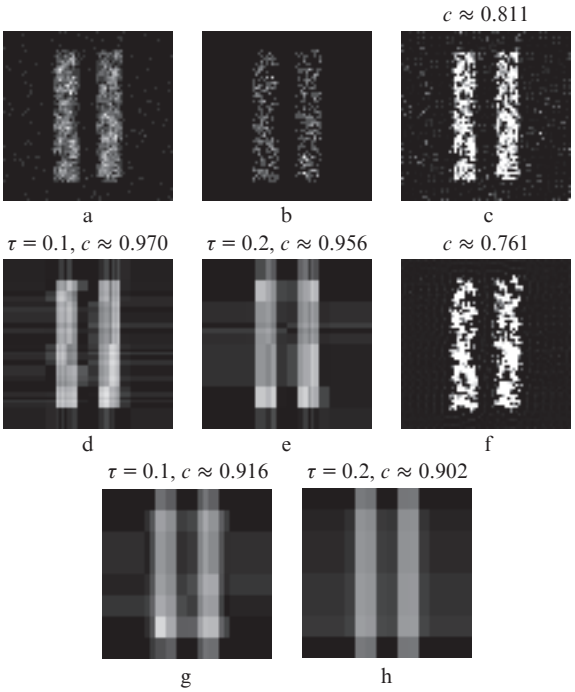

Figure 7. Quantum images of the object in Fig. 4a, recorded in (a) the object and (b) reconstruction channels, and the results of their processing by the reduction method: processing of both images (c) in the absence of sparsity information and (d, e) in the presence of such information, as well as (f–h) similar processing of a ghost image only. In contrast to Fig. 4, the quantum efficiencies of the detectors are 0.4 in the object channel and 0.2 in the reconstruction channel.

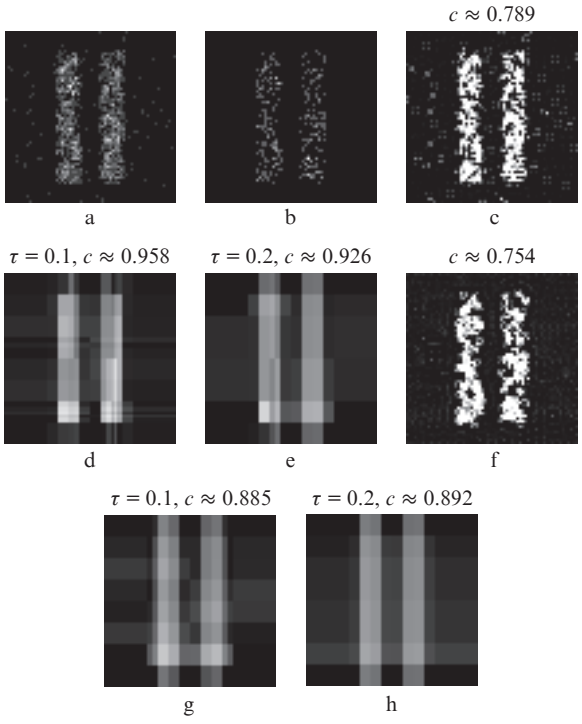

Figure 8. Quantum images of the object in Fig. 4a, recorded in (a) the object and (b) reconstruction channels, and the results of their processing by the reduction method: processing of both images (c) in the absence of sparsity information and (d, e) in the presence of such information, as well as (f–h) similar processing of a ghost image only. In contrast to Fig. 4, the quantum efficiencies of the detectors are 0.2.

ues of τ used in Fig. 4 are chosen so that in Fig. 4e the distortions are not noticeable yet, and in Fig. 4f they are already noticeable.

Comparison of Figs 4 and 5 confirms the above assumption that, if there is additional information, the gain due to processing the image recorded in the object channel decreases with its sign being unchanged. Attenuation of illumination, for which the error in the result of the reduction of a pair of images in the absence of sparsity information approximately corresponds to the error in the reduction of the ghost image before the illumination decrease, is smaller than that in Fig. 3. This is because the gain decreases when taking into account the information that the pixel transparency values belong to a unit segment, and the reduction errors decrease slightly more when using sparsity information than without using it.

The noise level of the estimate without using sparsity information constructed only from the ghost image (Fig. 4g) is greater than that constructed from both images (Fig. 4d). Therefore, at the same values of the parameter τ of the algorithm, which is responsible for the balance between blurring of important details of the image and noise suppression, the image blur is larger for the estimate constructed only from the ghost image: the estimates in Figs 4h and 4i are distorted to a greater extent than in Figs 4e and 4f.

Figures 6–8 show results similar to those shown in Fig. 4, but for different quantum efficiencies of sensors. As one would expect, at different sensor efficiencies in the object and reconstruction channels, the use of more efficient sensors in the object channel improves the reduction quality of the pair of resulting images (see Figs 6 and 7), but only slightly affects the quality of the reduction of the ghost image only. A decrease in the efficiency of detectors in the object channel with a fixed efficiency of detectors in the reconstruction channel faster degrades the quality of the reduction of the obtained pair of images than a decrease in the efficiency of detectors in the reconstruction channel solely, keeping it fixed in the object channel.

Figures 9 and 10 show simulation results similar to those shown in Fig. 4, with the number of noise photons decreased and increased by 10 times. As expected, an increase in the number of noise photons increases the error of the estimate constructed using both images and does not affect the error of the estimate constructed only from the ghost image due to the suppression of the contribution of noise photons by the coincidence circuit.

Figure 11 shows the simulation results for another object of study and with the different formalisation of sparsity information using the basis of the discrete cosine transform rather than the Haar basis of Figs 4–10. Due to the greater complexity of the new object, a larger average number of illuminating photons (10 photons per pixel) was used. In this case, it can be seen that despite the greater degree of overlap of the transparency distribution and its evaluation when processing only the ghost image, Fig. 11i is blurred stronger than Fig. 11f.

Finally, the localisation of noise caused by the use of the image obtained in the object channel differs from the localisation of noise associated with the non-unit efficiency of the detectors. While for the noise associated with noise photons the distribution over the image area, as a rule, is independent of the object, for the noise associated with the inefficiency of the detectors the distribution over the image area depends directly on the object, because the more photons reach the

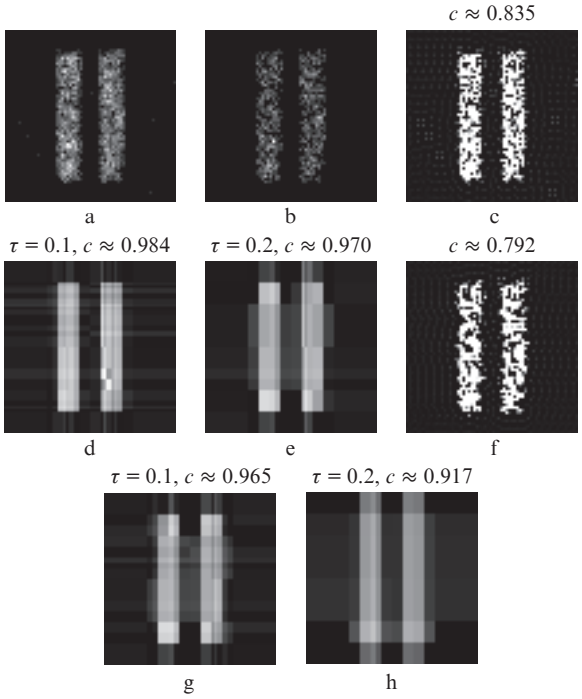

Figure 9. Quantum images of the object in Fig. 4a, recorded in (a) the object and (b) reconstruction channels, and the results of their processing by the reduction method: processing of both images (c) in the absence of sparsity information and (d, e) in the presence of such information, as well as (e–h) similar processing of a ghost image only. In contrast to Fig. 4, the average number of noise photons is reduced by a factor of 10 (to 0.01).

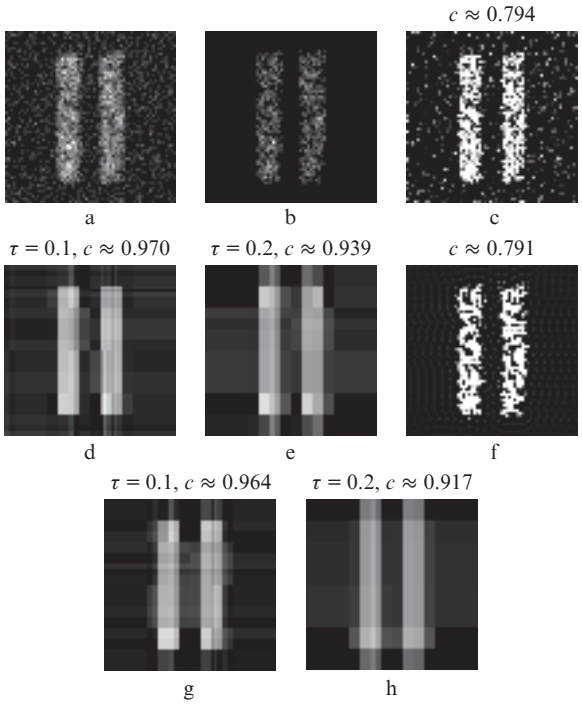

Figure 10. Quantum images of the object in Fig. 4a, recorded in (a) the object and (b) reconstruction channels, and the results of their processing by the reduction method: processing of both images (c) in the absence of sparsity information and (d, e) in the presence of such information, as well as (e–h) similar processing of a ghost image only. In contrast to Fig. 4, the average number of noise photons is increased by 10 times (up to 1).

sensor, the greater the variance of the photocounts. Therefore, a change in the parameter τ differently affects the distortion of image details located in areas with different average brightness.

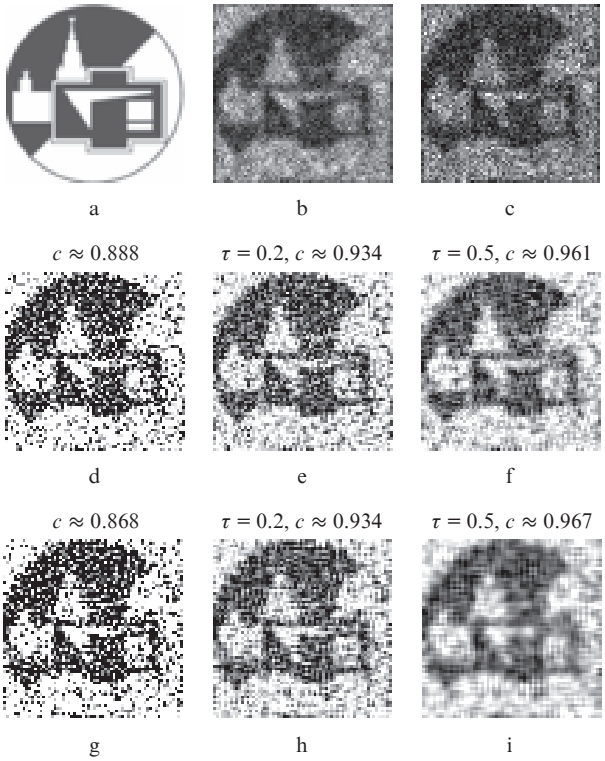

Figure 11. Quantum images of (a) the object recorded in (b) the object and (c) reconstruction channels, and the results of their processing by the reduction method: processing of both images (d) in the absence of sparsity information and (e, f) in the presence of such information, and also (g–i) similar processing of a ghost images only. In contrast to Figs 4–10, to formalise sparsity information the basis of the discrete cosine transform was used rather than the Haar basis.

5. Conclusions

The results of computer simulation show that, with non-unit efficiency of sensors, the registration of an additional image in the object channel allows extracting additional information from the object at a fixed illumination intensity. In the case of a sufficiently good quality of the result of processing only a ghost image, registration of an additional image allows a reduction of the illumination intensity preserving the quality of the processing result.

Note that the considered image registration scheme allows improving the quality of the quantum image at the stage of computer processing also by taking into account the diffractional limitations of ghost images [16–18]. This is because a conventional image is not subject to diffraction limitations present in ghost images and associated with the limited transverse dimensions and, therefore, the divergence of the pump beam. The study of the influence of diffraction, as well as the case when the instrument functions of the sensors are different, is a subject of further research.

Acknowledgements. This work was supported by the Russian Foundation for Basic Research (Grant No. 18-01-00598 A).

References

1. Kolobov M.I. (Ed.) *Quantum Imaging* (New York: Springer-Verlag, 2007; Moscow: Fizmatlit, 2009).
2. Treps N., Delaubert V., Maître A., et al. *Phys. Rev. A*, **71** (1), 013820 (2005).
3. Pyt'ev Yu.P. *Metody matematicheskogo modelirovaniya izmeritel'no-vychislitel'nykh sistem* (Methods of Mathematical Modelling of Measuring-Calculating Systems) (Moscow: Fizmatlit, 2012).
4. Balakin D.A., Pyt'ev Yu.P. *Moscow Univ. Phys. Bull.*, **72** (2), 101 (2017) [*Vestn. Mosk. Univer., Ser. Fiz. Astronom.*, (2), 3 (2017)].
5. Balakin D.A., Pyt'ev Yu.P. *Uchen. Zap. Fiz. Fak-ta Mosk. Un-ta*, (5), 1850301 (2018).
6. Balakin D.A., Belinsky A.V., Chirkin A.S. *JETP*, **125** (2), 210 (2017) [*Zh. Eksp. Teor. Fiz.*, **152** (2), 252 (2017)].
7. Morris P.A., Aspden R.S., Bell J.E.C., et al. *Nat. Commun.*, **6**, 5913 (2015).
8. Shi X., Huang X., Nan S., et al. *Laser Phys. Lett.*, **15** (4), 045204 (2018).
9. Gong W., Han S. *Sci. Rep.*, **5** (1), 9280 (2015).
10. Zerom P., Chan K.W.C., Howell J.C., Boyd R.W. *Phys. Rev. A*, **84** (6), 061804 (2011).
11. Katz O., Bromberg Y., Silberberg Y. *Appl. Phys. Lett.*, **95** (13), 131110 (2009).
12. Balakin D.A., Belinsky A.V. *Moscow Univ. Phys. Bull.*, **74** (1), 8 (2019) [*Vestn. Mosk. Univer., Ser. Fiz. Astronom.*, (1), 10 (2019)].
13. Balakin D.A., Belinsky A.V., Chirkin A.S. *Quantum Inf. Process.*, **18** (3), 80 (2019).
14. Mertens L., Sonnleitner M., Leach J., et al. *Sci. Rep.*, **7**, 42164 (2017).
15. Balakin D.A. *Mater. Mezhdunar. molodezhnogo nauchnogo foruma "Lomonosov-2019"* (Proc. Int. Youth Scientific Forum 'Lomonosov-2019') (Moscow: MAKS Press, 2019)].
16. Belinsky A.V., *Moscow Univ. Phys. Bull.*, **73** (5), 447 (2019) [*Vestn. Mosk. Univer., Ser. Fiz. Astronom.*, (5), 3 (2018)]; https://lomonosov-msu.ru/archive/Lomonosov_2019/data/section_33_16292.htm.
17. Moreau P.-A., Morris P.A., Toninelli E., et al. *Sci. Rep.*, **8** (1), 13183 (2018).
18. Moreau P.-A., Morris P.A., Toninelli E., et al. *Opt. Express*, **26** (6), 7528 (2018).